

Energetic Intra-Cloud Lightning in the RELAMPAGO Field Campaign

Andre Lucas Antunes de Sa¹, Robert Andrew Marshall¹, and Wiebke Deierling²

¹University of Colorado Boulder

²UCAR

November 22, 2022

Abstract

A particular strength of lightning remote sensing is the variety of lightning types observed, each with a unique occurrence context and characteristically different emission. Distinct energetic intra-cloud (EIC) lightning discharges – compact intra-cloud lightning discharges (CIDs) and energetic intra-cloud pulses (EIPs) – produce intense RF radiation, suggesting large currents inside the cloud, and they also have different production mechanisms and occurrence contexts. A Low-Frequency (LF) lightning remote sensing instrument array was deployed during the RELAMPAGO field campaign in west central Argentina, designed to investigate convective storms that produce high-impact weather. LF data from the campaign can provide a valuable dataset for researching the lightning context of EICs in a variety of sub-tropical convective storms. This paper describes the production of an LF-CID dataset in RELAMPAGO, and includes a preliminary analysis of CID prevalence.

Geolocated lightning events and their corresponding observed waveforms from the RELAMPAGO LF dataset are used in the classification of EICs. Height estimates based on skywave reflections are computed, where pre-fit residual data editing is used to improve robustness against outliers. Even if EIPs occurred within the network, given the low number of very high peak current events and receiver saturation, automatic classification of EIPs may not be feasible using this dataset. The classification of CIDs, on the other hand, is straightforward and their properties, for both positive and negative polarity, are investigated. A few RELAMPAGO case studies are also presented, where high variability of CID prevalence in ordinary storms and high-altitude positive CIDs, possibly in overshooting tops, are observed.

Hosted file

agusupporting-information.docx available at <https://authorea.com/users/533549/articles/598232-energetic-intra-cloud-lightning-in-the-relampago-field-campaign>

Energetic Intra-Cloud Lightning in the RELAMPAGO Field Campaign

A. Antunes de Sá¹, R. Marshall¹, W. Deierling^{1,2}

¹Smead Aerospace Engineering Sciences Department, University of Colorado Boulder, Boulder, CO, USA

²National Center for Atmospheric Research, Boulder, Colorado, USA

Key Points:

- Classification and height estimation of Energetic Intra-Cloud Lightning is investigated using RELAMPAGO LF lightning waveforms
- A small number of high-peak current events and saturation of LF receivers hinders the observation of Energetic In-Cloud Pulses in RELAMPAGO
- A catalog of RELAMPAGO Compact Intra-Cloud Discharges is produced to be used in future study of their occurrence in different storm types

Corresponding author: André L. Antunes de Sá, andre.antunesdesa@colorado.edu

Abstract

A particular strength of lightning remote sensing is the variety of lightning types observed, each with a unique occurrence context and characteristically different emission. Distinct energetic intra-cloud (EIC) lightning discharges – compact intra-cloud lightning discharges (CIDs) and energetic intra-cloud pulses (EIPs) – produce intense RF radiation, suggesting large currents inside the cloud, and they also have different production mechanisms and occurrence contexts. A Low-Frequency (LF) lightning remote sensing instrument array was deployed during the RELAMPAGO field campaign in west central Argentina, designed to investigate convective storms that produce high-impact weather. LF data from the campaign can provide a valuable dataset for researching the lightning context of EICs in a variety of sub-tropical convective storms. This paper describes the production of an LF-CID dataset in RELAMPAGO, and includes a preliminary analysis of CID prevalence.

Geolocated lightning events and their corresponding observed waveforms from the RELAMPAGO LF dataset are used in the classification of EICs. Height estimates based on skywave reflections are computed, where pre-fit residual data editing is used to improve robustness against outliers. Even if EIPs occurred within the network, given the low number of very high peak current events and receiver saturation, automatic classification of EIPs may not be feasible using this dataset. The classification of CIDs, on the other hand, is straightforward and their properties, for both positive and negative polarity, are investigated. A few RELAMPAGO case studies are also presented, where high variability of CID prevalence in ordinary storms and high-altitude positive CIDs, possibly in overshooting tops, are observed.

1 Introduction

Lightning remote sensing provides crucial information in the research of thunderstorms and associated phenomena, where its significance lies in the variety of lightning types, often with a unique occurrence context and characteristically different electromagnetic emissions. Of these lightning types, cloud-to-ground (CG) lightning has been historically the most studied, because of a more direct impact on society and higher data availability, and it has been associated with high-energy emissions in the upper atmosphere above thunderstorms (Inan et al., 2010), such as sprites (Franz et al., 1990) and elves (Inan et al., 1991; Fukunishi et al., 1996). But interest on energetic intra-cloud (EIC)

45 classes, i.e., compact intracloud discharges and energetic in-cloud pulses, has been grow-
46 ing in the last couple of decades, accompanied by a greater understanding of the phys-
47 ical process behind them and their connection to other lightning-related phenomena, such
48 as fast breakdown and Terrestrial Gamma-Ray Flashes (TGFs).

49 Compact Intracloud Discharges (CIDs), also known as Narrow Bipolar Events (NBEs)
50 or Narrow Bipolar Pulses (NBPs) based on their radio emission signatures, were first re-
51 ported in the 1980s (Vine, 1980; Willett et al., 1989) and were remarked as strong emit-
52 ters of HF-VHF radiation characterized by bipolar narrow electric field pulses (10-20 μ s).
53 The term CID was coined later by Smith et al. (1999a), who associated the NBEs to other
54 classes of intracloud discharges and inferred their relatively small spatial extent of hun-
55 dreds of meters. CIDs were also found to occur either in isolation from other discharges
56 in a storm or as the initiating event of an IC flash (Rison et al., 1999). Smith et al. (1999a)
57 also noted that the events were so different from other lightning phenomena, that a novel
58 type of discharge mechanism seemed to be required to explain them, while (Eack, 2004)
59 stated that even if the breakdown mechanism was the same, with streamers or lightning
60 leaders, the CID impulsive nature and high peak RF power made them distinct from con-
61 ventional lightning.

62 Even after four decades of study, there is still no consensus on the mechanisms re-
63 sponsible for CIDs, though that is quickly changing. A possible mechanism based on a
64 relativistic runaway electron avalanche (RREA), seeded by an extensive atmospheric shower
65 (EAS) of cosmic rays, was introduced by A. Gurevich et al. (2004) and A. V. Gurevich
66 and Zybin (2005). Following the same RREA-EAS theory, Watson and Marshall (2007)
67 used a modified transmission line model and an exponentially increasing current with
68 altitude to show agreement with electric field change measurements of CIDs. Nag and
69 Rakov (2010) then explained the radio signature of CIDs, particularly their secondary
70 peaks, with a bouncing wave model, where the current oscillates between the two ends
71 of the short channel associated with CIDs. In contrast, Arabshahi et al. (2014) showed
72 that thunderstorm electric fields and cosmic ray energies required to match measured
73 CIDs with the RREA-EAS model were not realistic. Finally, Rison et al. (2016) proposed
74 that CIDs are caused by a type of fast positive breakdown, a precursor mechanism they
75 suggest is associated with all ICs and possibly CG lightning flashes, which was supported
76 by Liu et al. (2019); Tilles et al. (2019) additionally observed fast negative breakdown
77 producing CIDs as well.

78 Another distinct class of energetic ICs, Energetic In-cloud Pulses (EIPs), were iden-
79 tified by Lyu et al. (2015). Suggested by the bimodal distribution of the impulse charge
80 moment change (iCMC) for high peak current lightning (Cummer et al., 2013), there was
81 already strong indication that other high peak current IC events, besides CIDs, might
82 be able to emit strong RF radiation. In contrast to CIDs, EIPs last an order of magni-
83 tude longer and are not isolated, spatially or temporally, but instead are associated with
84 smaller discrete pulses within its associated time window, generally embedded in other
85 electrical activity during a storm. Furthermore, in an analysis of a sample of CIDs and
86 EIPs occurring over 44 days in the fall in the Southeastern USA, Lyu et al. (2015) in-
87 ferred that while negative CIDs were generated at 16–19km altitude, considered to be
88 the strongest convection altitude during storms, between the upper positive and nega-
89 tive screening charge layers in a standard tripole storm, the positive EIPs were produced
90 at 10–13km within a weaker convection region between the main negative and upper pos-
91 itive charge layers. Both positive and negative EIPs have been associated with a differ-
92 ent subset of Terrestrial Gamma-Ray Flashes (TGFs) (Lyu et al., 2015, 2016, 2018; Lyu
93 & Cummer, 2018), the strongest source of natural radiation on Earth occurring above
94 thunderstorms in the upper atmosphere; the EIP-TGF association indicates that they
95 may be linked by the same production mechanism. A link between elves, EIPs, and TGFs
96 has also been suggested (Liu et al., 2017).

97 The EIP production mechanism is associated with the propagation of negative lead-
98 ers, upward leaders with +EIPs and more rarely downward leaders with -EIPs, though
99 it was originally not clear if EIPs were energetic leaders themselves. Recent radio inter-
100 ferometry observations provide clarification on the leader-EIP-TGF connection, and sug-
101 gest that EIPs are generated by the relativistic discharge responsible for an accompa-
102 nying TGF, rather than by streamer or leader activity (Tilles et al., 2020). The EIP pro-
103 duction mechanism is thus markedly different from that of CIDs, as also indicated by
104 the different temporal and spatial context in which they occur.

105 In this paper, EICs from different storms during the RELAMPAGO field campaign
106 are investigated. Classification of EIC lightning types is described and validated, with
107 supporting VHF and E-field change data available during the campaign. The prevalence
108 of EICs and some of their properties during RELAMPAGO storms are discussed.

2 Background

2.1 RELAMPAGO Field Campaign

The Remote sensing of Electrification, Lightning, And Mesoscale/Microscale Processes with Adaptive Ground Observations (RELAMPAGO) field campaign was conducted from November to mid-December 2018, parts of the campaign started earlier in 2018 and extended through early 2019 in west central Argentina, in the vicinity of the Sierras de Córdoba and near the city of Mendoza at the foothills of the Andes mountains. Primarily funded by the National Science Foundation, this campaign was an international collaboration seeking to observe and investigate convective storms that produce high-impact weather (Nesbitt, 2020). This region of Argentina is known to exhibit some of the most intense storms in the world as well as the highest lightning flash rate per storm system (Zipser et al., 2006; Cecil et al., 2015). An association of severe weather with storms occurring in this region is supported by radiometer observations (Cecil & Blankenship, 2012) and public reports (Rasmussen et al., 2014).

The RELAMPAGO campaign incorporated a multitude of instrument types, particularly during the intensive observation period between November 1 and December 15, 2018. Lightning-observing instrumentation included an array of four Very Low Frequency/Low Frequency (VLF/LF) autonomous magnetic sensors (LFAMS or “LF instrument”) deployed by the University of Colorado Boulder; an 11 station Lightning Mapping Array (LMA; T. J. Lang et al., 2020) deployed by NASA’s Marshall Space Flight Center, an array of eight electric field mills (EFMs; Antunes de Sá et al., 2020) deployed by the University of Colorado Boulder, and an array of 8 field change meters (CAMMA; Zhu et al., 2020) deployed by the University of Alabama Huntsville. Many other instruments were deployed or operating during the campaign, including radars, hail pads, and soundings; see Nesbitt (2020) for a full list of deployed instrumentation and an overview of the field campaign. This paper makes use of the geolocated lightning data from the LF instruments (Antunes de Sa et al., 2021). Other RELAMPAGO datasets are also used in this investigation on RELAMPAGO EICs, including the LMA (T. Lang, 2020) and CAMMA datasets (Zhu et al., 2020; Carey et al., 2019a, 2019b). Unaffiliated datasets that observed RELAMPAGO storms are also used, such as from NOAA’s Geostationary Operational Environmental Satellite R series (GOES-R) Advance Baseline Imager (ABI; GOES-R Calibration Working Group & GOES-R Program Office, 2017) and Geostationary Light-

141 ning Mapper (GLM; GOES-R Series Program, 2019) instruments, and from the Earth
142 Networks Total Lightning Network (ENTLN; Heckman, 2014).

143 **2.2 RELAMPAGO LF Data Products**

144 A brief overview of the deployed LF system and LF datasets that are used in this
145 study to identify various lightning types is provided below. More detailed information
146 about these datasets can be found in Antunes de Sa et al. (2021).

147 The LF instruments deployed in the RELAMPAGO campaign are based on the 100
148 kHz sampling rate VLF instrument described by (M. Cohen et al., 2010), with the proper
149 modifications for operating at 1 MHz sampling rate and collecting VLF/LF (3–400 kHz)
150 data. The instrument’s antenna element consists of two air-core magnetic loop anten-
151 nas, aligned with North-South (Channel 1) and East-West (Channel 2) direction. The
152 instrument continuously records radio signals arriving at the antennas, referred to as the
153 LF Level 0 (raw) dataset. Two data products have been released after hierarchical pro-
154 cessing of the raw data. The Level 1 dataset (Deierling et al., 2019) is a station-specific
155 collection of lightning waveform data (radio atmospherics or sferics) extracted from the
156 Level 0 data. The Level 2 data product (Deierling et al., 2021) provides information on
157 geolocated lightning events and lightning flashes from the Level 1 sferic observations. A
158 detailed description of the instrument, RELAMPAGO deployment, and data process-
159 ing can be found in the accompanying documentation to the data products at the ref-
160 erences provided.

161 **2.2.1 Level 1 Data Product**

162 The processing for this data product mainly consists of a peak magnitude search
163 for sferics across the raw data (quadrature addition of the two channels) with a peak stronger
164 than five times the raw data noise floor. Once a possible sferic has been identified, a data
165 window of 1.2 ms is extracted from both channels with the main peak centered at 200
166 μ s. Power-line noise at 50 Hz and harmonics is removed from the data using filtered us-
167 ing a “Humstractor” algorithm (M. B. Cohen et al., 2010). Fig. 1 presents an illustra-
168 tion of the propagation paths from a typical lightning emission, an example Level 1 sferic
169 from the LF1 receiver, and waveform features used in Section 3.1 for EIC classification.

170

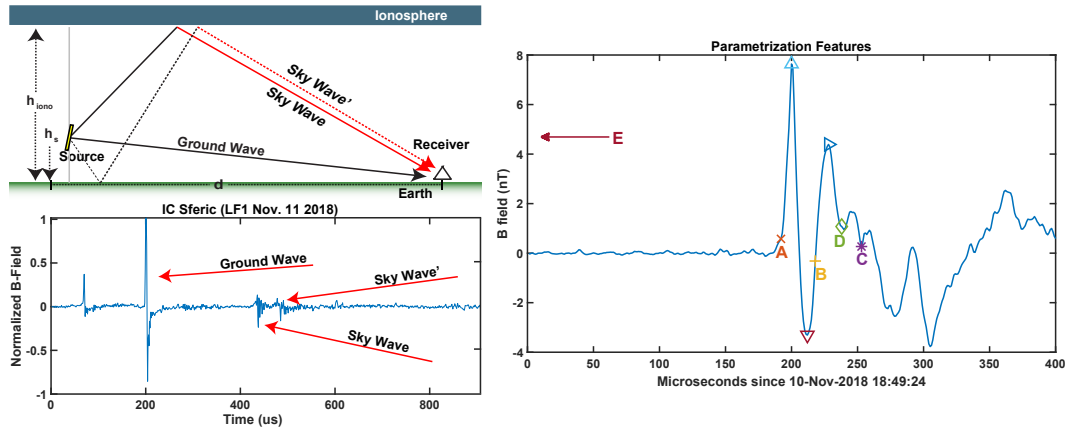


Figure 1. Illustrations of the lightning emission propagation path towards the receiver, using a simplified flat-earth assumption, adapted from (Marshall et al., 2015) (top), an IC sferic received by LF1 during RELAMPAGO (bottom), and waveform features *A* through *E* used in the EIC parametrization suggested by (Lyu et al., 2015) (right). The paths illustrated and identified in the sferic include a ground wave, propagated directly between source and observer, and sky waves, ionospheric reflections. The ground-ionospheric path is only observed for intra-cloud, where the source height is larger than zero. Paths with more hops are also possible but are rarely observed due to stronger attenuation.

171

2.2.2 Level 2 Data Product

172

173

174

175

176

177

178

179

180

181

182

183

184

185

The Level 2 data processing, summarized in Fig. 2, involves matching the Level 1 sferics, using cross-correlations, into lightning events and extracting time-of-arrival observations for geolocation. Geolocation is accomplished using a linearized least-squares filter, which assumes an unbiased gaussian distribution of time of arrival uncertainty of $10\ \mu\text{s}$, a spherical time-of-arrival model, and negligible model and linearization errors. The time of arrival uncertainty is a best guess based on the station clock error correction performed at an earlier stage. To ensure the linearization assumption, a low-precision *a priori* is generated using the non-linear time-of-arrival model and subsequently fed into the least squares filter. Peak current is estimated using peak magnitude observations of an event and an attenuation model based on finite-difference time-domain (FDTD) simulations of lightning propagation (Marshall, 2012), under the assumption that a known peak radiated field a distance away from the source, e.g., 100 km, is proportional to the source's peak current by a constant parameter (Orville, 1991). Peak current estimates are set to infinity for events that saturated all observing receivers. A domain mask is used

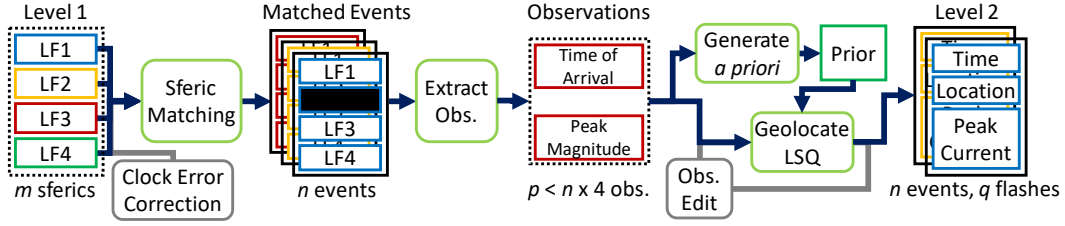


Figure 2. Flowchart describing the geolocation data processing for generating the Level 2 data product. The gray ad-hoc processes are only necessary in handling specific issues with the RELAMPAGO dataset.

186 to discard geolocated events outside the observable region of the LF array, which varies
 187 depending on which LF stations made an observation for a specific event. A quality mea-
 188 sure is computed at the matching step for each event based on the minimum cross-correlation
 189 score across its sferics. Additionally, geolocated events are clustered into lightning flashes
 190 based on a spatiotemporal distance criteria of 10 km to the flash centroid and 0.3 s to
 191 the last event of a flash.

192 3 Event Processing

193 3.1 EIC Classification

194 Automatic classification of CID sferics was first demonstrated by Smith et al. (2002),
 195 leveraging the fast rise and fall times of the CID pulse and temporal isolation from other
 196 VLF/LF emissions from lightning processes. Smith et al. (2002) showed that in the two-
 197 parameter space of rise-plus-fall time and signal-to-noise ratio, the distinction between
 198 the CID and non-CID population was strong enough to allow for a criterion-based clas-
 199 sification (See Fig. 14, Smith et al., 2002). Similarly, following the discovery of EIPs, Lyu
 200 et al. (2015) proposed a CID/EIP classification scheme based on three time-domain pa-
 201 rameters: pulse width (related to rise-plus-fall time), peak ratio (ratio between opposite
 202 polarity peaks in bipolar EIC pulses), and isolation ratio (related to signal-to-noise ra-
 203 tio). Lyu et al. (2015) manually identified CIDs and EIPs in 44 days of storms in the
 204 southern United States during the fall season, and also found a distinction between the
 205 lightning type populations. Note that Lyu et al. also implicitly used peak current and
 206 CG-IC type as extra classification parameters, only classifying lightning events with a

207 National Lightning Detection Network (NLDN) peak current estimate higher than 200 kA
 208 and categorized by NLDN as IC lightning.

209 The three-parameter classification suggested by Lyu et al. (2015) is adopted in this
 210 paper, with implementation details and changes described in this section. The RELAM-
 211 PAGO LF geolocated events data (Level 2 data), which provide time, location, and peak
 212 current, in conjunction to the corresponding LF sferic observations for each event (Level
 213 1 data) are used. The classification is applied directly to all of the LF data in RELAM-
 214 PAGO, without peak current or CG-IC type constraints, and peak current is used as a
 215 fourth parameter in classification. The 200 kA requirement in Lyu et al. (2015) is restric-
 216 tive in order to collect only “highly energetic” ICs, and they acknowledge that the NLDN
 217 peak current estimate, which is effectively a scaled and normalized peak radiated elec-
 218 tric field also used in the RELAMPAGO LF data, is not a well calibrated measurement
 219 for IC lightning.

The classification parameters are derived from key features of the observed sferic waveform, per Lyu et al. (2015) and illustrated in Fig. 1: *A* preceding the initial peak and at 10% of its maximum value; *B* following the main peak and at 10% of its maximum; *C* following the overshoot peak and at 10% its maximum; *D* at 20 μ s after *B*, and *E* approximately 500 μ s preceding *A*. The parameters are then defined per Lyu et al. (2015) as follows: pulse width is the duration of the pulse, the time duration between *A* and *C*; the peak ratio is the ratio between the first peak in the sferic pulse (initial peak) and the second peak in the pulse (main peak), in the *AB* window; and isolation ratio is the sum of the preceding- and post-activity ratios. This activity ratio γ is defined in Eq. 1 with the top sum over points in the window *AB*, and the bottom sum over points in the window *EA* for preceding activity or over points in the window *BD* for post activity:

$$\gamma = 10 \times \log_{10} \left[\frac{\frac{1}{M} \left(\sum_{i=1}^M B_i^2 \right)}{\frac{1}{N} \left(\sum_{j=1}^N B_j^2 \right)} \right] \quad (1)$$

220 Our specific implementation of the waveform feature extraction relies on positive
 221 identification of the initial, main and overshoot peaks, and includes basic quality con-
 222 trol. The identification of the initial peak, which is the most important feature for suc-
 223 cessful EIC classification since all other features depend on it, actually starts in the Level
 224 2 data processing. In the Level 1 data, the 1.2 ms extracted sferic has its highest peak
 225 centered at the 200th μ s, but it often does not capture the initial peak of the sferic. For

226 identification of the initial peak only, the sferic is filtered by a lowpass IIR 12-order but-
227 terworth filter with cutoff frequency at 10 kHz and the first peak in the window is se-
228 lected to be the initial peak at the 200th μs , correctly capturing pulses with a weaker
229 groundwave. A cross-correlation score is computed for different sferic observations of the
230 same event, and bad matches, including those with poor alignment, are reflected in this
231 score for later quality control. The applied shifts to the Level 1 data are reported in the
232 Level 2 geolocation process. In the classification algorithm, with the applied shifts to the
233 sferics, the initial and main peaks are found to be the minimum and maximum peaks
234 respectively, or vice-versa for negative polarity pulses, in the 150–250 μs window of the
235 sferic. Both bipolar and unipolar pulses are captured, by setting the first peak to be the
236 initial peak but only if it's smaller (greater) than 10% of the second peak, which is al-
237 ways true for bipolar pulses and only true for unipolar pulses with the initial peak be-
238 ing greatest in magnitude. This also limits all unipolar pulses to a peak ratio of at most
239 10. Note that EICs are bipolar, with possible overshoots. A and B are then picked to
240 be the first point in time that satisfy the criteria in the previous paragraph, with B not
241 exceeding 100 μs from the main peak. The overshoot peak is found to be the next opposite-
242 polarity peak within 30 μs of B , and again C is picked in the 35 μs window after the over-
243 shoot peak. If the overshoot peak or C cannot be found, C is set to be the same as B .
244 For any other feature that cannot be found to satisfy the criteria, the classification is dis-
245 carded. Note that the window limits are all within what is expected of EIC waveforms,
246 but it is biased against the slowest CG waveforms. Also note that E is set to the begin-
247 ning of the sferic record, which is at most 200 μs before the initial peak, and the clas-
248 sification is discarded if E is less than 100 μs before A to avoid overestimation of the iso-
249 lation ratio.

250 With the classification parameters computed for every sferic observed for each event
251 (maximum of 4 sferics per event, from our 4 LF receivers), the parameter's averages are
252 used in the EIC classification. Because receiver saturation affects the observations, es-
253 pecially for higher peak current events close to the stations, observations from saturated
254 sferics are not used in the parameter's averages. If all stations saturated, the parame-
255 ter from LF4 was used due to that station's much higher saturation point. Other saturation-
256 related issues include some underestimation of high peak currents or the inability to com-
257 pute peak current for very strong events, which are reported in the LF level 2 data with

258 an “infinite” peak current. In the worst-case, saturation can cause heavy distortion of
 259 the sferic waveform, preventing successful matching and geolocation.

260 In order to capture the strongest high peak-current events, possibly not captured
 261 in the LF level 2 data, ENTLN pulse data (analogous to LF Level 2 events) with reported
 262 peak-currents higher than 100 kA are matched to RELAMPAGO LF Level 1 data and
 263 used in the classification of these events. Note that this relaxes the Level 2 event require-
 264 ment of having at least 3 sferic observations for an event, as one sferic is enough for an
 265 ENTLN-based event to be classified. A large number of ENTLN events are actually in
 266 the LF Level 2, some with under-estimated peak currents, some with similar peak cur-
 267 rents, and most with peak current set to infinity due to saturation. To avoid duplicat-
 268 ing the events, the matching ENTLN pulse information replaces those LF Level 2 event
 269 entries. A match is considered when an ENTLN event is within 0.5 ms of sferics used in
 270 an LF event entry, corrected for the propagation delay expected from the ENTLN-reported
 271 source location to our LF receivers. About half of the ENTLN events are seen in the LF
 272 data, with periods of higher LF loss such as November 10 and 11, and other times with
 273 more matches. Of all the events to be classified, i.e., LF events with peak-currents higher
 274 than 10 kA, only a small percentage, <1%, are taken from ENTLN 100+ kA.

275 3.2 EIC Height

Given the geometry of the lightning emissions, ground and reflected skywaves (Fig. 1), it is possible to estimate the lightning source height for ICs. Although the reflection mechanism at the ionosphere is more complicated than a perfect reflection, the assumption is acceptable within the uncertainties discussed here. Smith et al. (1999a) derived a flat-earth model of the skywave reflection geometry with the 1-hop ground-skywave delays, Δt for source-ionosphere and $\Delta t'$ for source-ground-ionosphere, given by:

$$\begin{aligned}\Delta t c &= \sqrt{d^2 + (2h_{\text{iono}} - h_s)^2} - \sqrt{d^2 + h_s^2} \\ \Delta t' c &= \sqrt{d^2 + (2h_{\text{iono}} + h_s)^2} - \sqrt{d^2 + h_s^2},\end{aligned}\tag{2}$$

276 where d is the great-circle distance between source and receiver, h_{iono} is the ionosphere
 277 reflection height, h_s is the source height, and c is the speed of light. This model is sim-
 278 ple yet useful and has been used in CID height estimates (e.g., Wu et al., 2011, 2012),
 279 though a slightly more complicated spherical Earth method has also been used exten-
 280 sively (e.g., Smith et al., 2004; Zhang et al., 2016). The flat-earth assumption produces

281 a model error below 300 m for the source height estimate, which is much smaller than
282 the uncertainty caused by the location precision of a few kilometers.

283 The skywave delay observations are extracted from the sferic records by finding the
284 two strongest positive and two strongest negative peaks after the waveform feature D .
285 The first of four peaks is checked to be followed by the opposite polarity peak within 20 μs .
286 The groundwave initial or main peak is then subtracted from the skywave peaks, accord-
287 ing to the order in which they appear in the sferic, i.e., first peak of a skywave is sub-
288 tracted by the initial peak and second peak of skywave, if it exists, is subtracted by the
289 main peak. At best, each sferic yields 4 observations, if none are discarded throughout
290 the process.

291 The source height and ionosphere height can then be estimated using the obser-
292 vations, which form an over-determined system when more than 2 observations are ac-
293 quired. A statistical linear least squares is employed in estimating the heights, with an
294 assumed normal observation uncertainty of 2 μs for each delay, estimated empirically from
295 the observation detection and timing errors. Note that the uncertainty in the observa-
296 tion pairs from the same sferic are not independent, and violating that assumption leads
297 to slight underestimation of height uncertainty. An *a priori* is given to the filter with
298 source height 10 km, and ionosphere height between 88 km (night) and 73 km (day), with
299 a fast transition during twilight, based on ionosphere height estimates in (Fig., 6 Smith
300 et al., 2004) and the RELAMPAGO dataset. Since there is a large contribution of erroneously-
301 detected skywaves which provide inaccurate height estimates, and the ionospheric height
302 can be reasonably constrained, a data editing scheme is employed based on the filter in-
303 novation, i.e., the pre-fit residual (observation-minus-expected). The mean innovation
304 is computed for a reflection pair, minimizing the source height dependence, and if it is
305 larger than 7.5 times the observation uncertainty of 2 μs (or 15 μs , roughly equivalent to
306 ± 4.5 km), that observation pair is discarded. Observation pairs that, by themselves, yield
307 IC heights less than 5 km or higher than 24 km are also discarded.

308 The innovation filter is highly successful in removing bad observations which could
309 otherwise greatly affect the height estimate, since the filter is not robust to bad obser-
310 vations. Observations from all stations are weighted the same even though at least one
311 station is likely to yield bad observations, e.g., depending on lightning location and the
312 fact that one pair of observations in a sferic is smaller and sometimes unidentifiable. In-

313 instead of removing stations, and only keeping the stronger reflection pair, the filter is able
 314 to utilize those observations when possible and increase estimate precision. For valida-
 315 tion, a plot of ionosphere height estimates from EICs during November 12, 2018 is shown
 316 in Fig. 3, where the method not only estimates a reasonable diurnal variation in the iono-
 317 sphere height, but also discards outliers and automatically selects the best observations
 318 to match the ionosphere height prior. Note that the innovation filtering has no direct
 319 impact on the source height estimate, except for the benefits of selecting the best ob-
 320 servations for its computations, and are allowed to vary significantly from its prior of 10 km
 according to the observation model, Eq. 2.

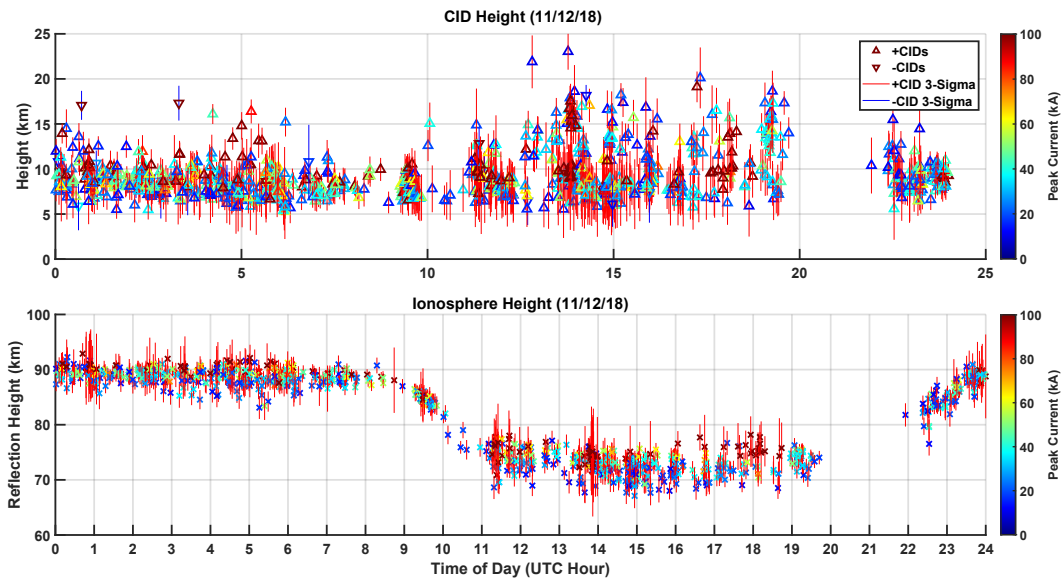


Figure 3. Plot of the CID and ionosphere height estimate that accompanies the height estimate of 1075 CIDs, of which a height estimate could be achieved for 947 CIDs, during RELAMPAGO storms on November 12 2018.

321

322 4 RELAMPAGO EICs

323 Classified EICs from the RELAMPAGO campaign are presented in this section and
 324 the classification results are investigated. There are about 100,000 lightning events col-
 325 lected by the LF system from select days during the RELAMPAGO campaign that were
 326 used in the classification. They are described in Table 1. Only events with an estimated
 327 peak current higher than 10 kA are classified, because the sferics associated with weaker

328 events and lower signal-to-noise ratio start to lose waveform features to the noise floor.
 329 To give context to the events, flash information for the same period is also presented,
 330 including flash rates, average flash peak current, I_{pk} , average multiplicity, and the po-
 331 sition in time of the highest peak current event in a flash, τ_{flash} , as a percentage. Flash
 332 peak current is reported as the maximum peak current of its constituent events, and τ_{flash}
 is only computed for flashes with multiplicity higher than one.

Table 1. RELAMPAGO LF events, with peak current higher 10 kA, used in the EIC classifica-
 tion and their average peak current, I_{pk} , are presented to the left for a selection of dates during
 the campaign. All RELAMPAGO LF flashes are also presented for context, including average
 flash peak current, multiplicity and the position in time of the highest peak current event in a
 flash, τ_{flash} , as a percentage.

Date	Events \geq 10 kA			Flashes				
	Count (#)	Rate (min^{-1})	I_{pk} (kA)	Rate (min^{-1})	Max Rate (min^{-1})	I_{pk} (kA)	Mult. (#)	τ_{flash} (%)
11/3/18	3861	2.68	17.27	5.45	74	6.76	3.31	59
11/10/18	15273	10.61	18.16	22.61	164	8.2	4.31	63
11/11/18	45731	31.76	16.67	53.26	499	8.56	5.07	67
11/12/18	22904	15.91	22.29	11.56	75	11.95	4.36	54
11/17/18	2324	8.64	17.04	8.59	22	8.91	2.98	64
11/26/18	3449	8.2	19.29	9.1	64	7.79	4.12	63
12/04/18	4709	3.27	18.6	5.8	77	7.22	3.92	55
All	98251	11.58	18.43	16.62	499	8.68	4.61	63

333
 334 Fig. 4 (top) shows the distribution of events on November 12, with the second high-
 335 est number of events reported and highest average peak current in a single day, in the
 336 classification parameter space. As expected, the population of CIDs, with low pulse width
 337 and high isolation ratio, is distinct from the rest of the distribution. A selection crite-
 338 ria of pulse width less than 50 μs , isolation ratio higher than 60 dB, and no criterion for
 339 either peak current or peak ratio is chosen for CIDs. EIPs, on the other hand, are much
 340 harder to identify. Since only very high peak current EIPs have been identified in the
 341 past, a peak current requirement is set for EIPs to record at least 200 kA of peak cur-
 342 rent, just as in Lyu et al. (2015). Also following the suggestions and discussions by Lyu

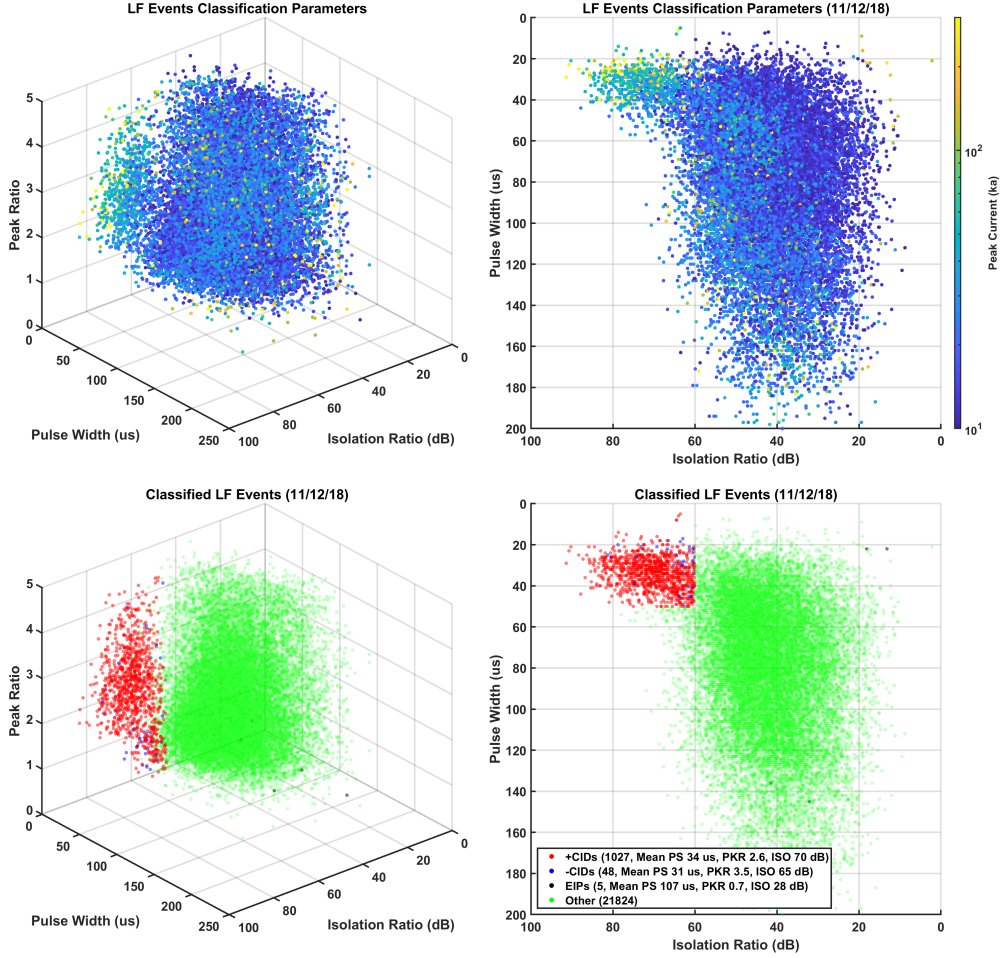


Figure 4. Distribution of RELAMPAGO LF events in the classification parameter space (top), i.e., pulse width (PS), peak ratio (PKR), isolation ratio (ISO), and peak current, and classified EIC LF events (bottom) on November 12 2018 for the whole day on November 12 2018. A low pulse-width high isolation population, expected for CIDs, is distinguishable from other events, in agreement with (Fig. 14, Smith et al., 2002) and (Fig. 1, Lyu et al., 2015). The population of EIPs, however, is not obvious.

343 et al. (2015), the EIP criterion for peak ratio is set to less than 1, i.e., main peak stronger
 344 than initial peak. Other criteria were not set given the already low number of potential
 345 EIPs, and so that more events could be investigated before being discarded.

346 The resulting EIC population after applying the selection criteria is shown in Fig. 4
 347 (bottom). Through manual validation of the sferic waveforms and against other RELAM-
 348 PAGO datasets such as from the LMA or CAMMA, we find that the criteria for CIDs,

349 used for all dates, successfully selects the CID population. Though the CID population
 350 changes slightly on different dates, with smaller pulse width average (faster), the 50 μ s
 351 criterion captures the slower events of that population when they exist, and the 60 dB
 352 criterion prevents non-CID events from being captured when the population is faster.
 353 As these criteria are relaxed, the number of false-positive CIDs quickly increases and true-
 354 positives decreases. Some true positives still exist outside the selection region due to er-
 355 rors in the computation of classification parameter, e.g., near-saturated/distorted spher-
 356 ics. With the chosen criteria, the number of CID false-positives is found to be small, <3%.

357 On the other hand, few potential EIP waveforms, if any, seem to agree to what is
 358 expected from past research. Most of the classified EIPs are actually highly saturated
 359 for all stations except LF4, and far enough away that the skywave blends with the ground-
 360 wave main peak, artificially deflating the peak ratio measure to fulfill the EIP selection
 361 criteria. This is obvious from many potential EIP waveforms with similar features, and
 362 the corresponding CAMMA record for one of these EIP candidates coincides to within
 363 1 ms and 5 km from two CAMMA sources near the ground, indicating a CG source. Ad-
 364 ditionally, the number of potential EIPs is very small, with just a handful occurring in
 365 well-observed RELAMPAGO storms and most at the edges of the LF observation region.
 366 Thus, this dataset might not be able to provide further insights into EIPs, aside from
 367 their supposed absence in the LF observed RELAMPAGO storms and classification com-
 368 plexity under saturated and distant receivers. As such, we focus the present analysis on
 369 CIDs.

370 Table 2 presents the properties associated with the classified CIDs, including preva-
 371 lence, average peak current, and source height. The most striking result is that the source
 372 height for +CIDs on November 10 is much higher than -CIDs. It is also accompanied
 373 by the smallest pulse widths recorded. The occurrence of the CID's was associated with
 374 several supercell storms that occurred that day, two of which are investigated in Section 5.
 375 November 12, characterized by a very large number of discrete non-severe storms, also
 376 displayed a large percentage of CIDs per storm, with one of these investigated in Sec-
 377 tion 5. Across all days, the source height distribution indicates higher altitudes for the
 378 rarer -CIDs than for +CID, as expected from past research, but not statistically sig-
 379 nificant given their uncertainties. A better understanding on the charge structure of the
 380 storms occurring on the investigated days is necessary for further conclusions about CID
 381 heights, some of which is provided in Section 5. The absence of CIDs on November 3 also

Table 2. Properties of classified positive and negative polarity CIDs classified from a selection of dates during the campaign. These include a total count of CID, the percentage of CIDs in the pool eligible events (Table 1), average peak current, average estimated source height (Section 3.2), average classification parameters pulse width (PS), peak ratio (PKR), isolation ratio (ISO), average multiplicity of its parent flash, and the average position in time of the CID within its parent flash, τ_{flash} , as a percentage.

+CIDs									
Date	Count (#)	Count (%)	I_{pk} (kA)	h_{s} (km)	PS (μs)	PKR (\circ)	ISO (dB)	Mult. (#)	τ_{flash} (%)
11/3/18	0	0	N/A	N/A	N/A	N/A	N/A	N/A	N/A
11/10/18	570	3.73	26.62	13.73	21.8	2.43	66.79	2.65	54
11/11/18	458	1.0	43.6	9.66	34.4	2.28	67.42	3.82	0.36
11/12/18	1027	4.48	44.27	9.31	34.07	2.58	70.47	3.55	24
11/17/18	63	2.71	19.45	9.07	35.22	1.62	63.75	2.78	55
11/26/18	97	2.81	24.7	8.83	35.25	2.07	69.34	4.82	39
12/04/18	78	1.66	17.16	9.82	37.51	1.31	63.74	4.82	41
All	2293	3.38	37.32	10.47	31.28	2.39	68.48	3.46	36
-CIDs									
Date	Count (#)	Count (%)	I_{pk} (kA)	h_{s} (km)	PS (μs)	PKR (\circ)	ISO (dB)	Mult. (#)	τ_{flash} (%)
11/3/18	1	0.03	13.14	N/A	29.5	1.35	66.42	3	0
11/10/18	131	0.86	21.39	11.17	28.84	2.07	65.78	3.31	68
11/11/18	101	0.22	18.8	12.14	27.54	2.51	63.73	4.19	56
11/12/18	48	0.21	26.48	9.96	30.8	3.45	65.24	2.9	31
11/17/18	17	0.73	17.16	9.96	27.41	1.44	63.33	2.12	45
11/26/18	33	0.96	16.23	8.63	27.99	2.83	63.52	3.27	44
12/04/18	34	0.72	20.4	10.05	30.75	1.95	63.55	3.18	35
All	365	3.73	20.56	10.86	28.77	2.40	64.62	3.43	53

382 needs to be investigated further for the individual storms on that day (not included in
 383 this study), given the similar count of LF events to November 17, 26 and December 4,
 384 which saw a much higher prevalence of CIDs. Finally, the distribution of τ_{flash} , the po-
 385 sition in time of the CID within its parent flash, shows enough variability to prevent strong
 386 conclusions. Overall, in our study +CIDs occur earlier in the flash, especially for flashes
 387 with low multiplicities. -CIDs occur later in the lifetime of a flash regardless of mul-
 388 tiplicity. This measure of τ_{flash} and multiplicity are highly affected by event detection
 389 efficiency (Antunes de Sa et al., 2021), which might explain some of the variability.

390 A supercell that occurred on November 10 is particularly useful in validating the
 391 classification because it occurred in the middle of the main RELAMPAGO instrument
 392 deployment region. As an example of the EIC validation capability for this dataset, Fig. 5
 393 shows the set of four LF sferics for an observed +CID, and an XLMA-style plot of CAMMA
 394 sources (LMA sources are also available). The sferic panel includes the classification fea-
 395 tures *A–D* explained in Section 3.1, as well as the skywave peak observations used in the
 396 source height estimate, explained in Section 3.2. Sferics from LF1, LF2, and LF3, all sat-
 397 urated to a certain extent, which certainly affected their waveform features, and so these
 398 were not used in the computation of the classification parameters. The identification of
 399 skywave peaks is also successful, yielding 3 pairs of observations for the ionosphere and
 400 source height estimates. Note that other observation pairs were erroneously identified
 401 (not shown) but subsequently discarded by the innovation filter. The XLMA-style plot
 402 shows the isolated CID (light blue triangle) occurred between two flashes, with a coin-
 403 ciding CAMMA source within 2 km in altitude, within the uncertainty of both sources.
 404 The EICs in this storm are investigated in the next section.

405 5 Storm Case-Studies

406 5.1 November 10, 2018, 19:30–22:30 UTC

407 The supercell storm of November 10, 2018, 19:30–22:30 UTC is one of the best RE-
 408 LAMPAGO examples for EIC research in terms of data availability. It displayed a rel-
 409 atively high number of CIDs, and was observed by most of the major RELAMPAGO in-
 410 struments, including radar sites.

411 Fig. 6 presents a map of the CID occurrence along with a time evolution panel dur-
 412 ing that storm. The two maps at the top of Fig. 6 display the locations of identified EICs

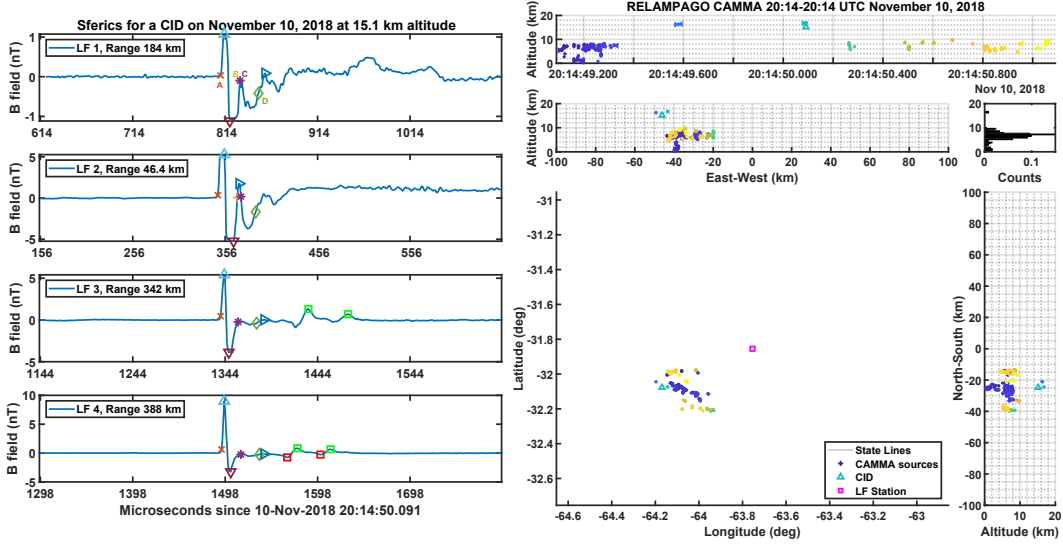


Figure 5. Panel of the LF sferics observed for a +CID (left) and XLMA-style plot of CAMMA sources (right). Sferic features A–D, initial, main and overshoot peaks, as well as skywave peaks (green and red squares) are displayed. On the right, CAMMA sources are color coded by time and flash boundaries are depicted using right- and left-pointing triangles in the top plot.

413 (left map), and locations of all LF flashes for this storm (right map), with markers color-
 414 coded by UTC time. The location markers are overlaid on ABI data for 22:05 UTC. The
 415 time evolution panel, below the maps, contains four plots. From top to bottom, the first
 416 plot shows EIC and LF flash rates (#/minute), the second plot shows the distribution
 417 of flash peak current, the third and fourth plots show a height distribution of all LMA
 418 sources in linear and log scales. Also on the third plot, +CID (red) and –CID (blue) source
 419 heights (circles) and coinciding LMA source heights (crosses) within 1 ms and 25 km are
 420 overlaid on the LMA height distribution. Before 20:40 UTC, only six LMA stations were
 421 operating, which is responsible for low detection efficiency, but a seventh station went
 422 online after that time providing higher quality data. Two animations are provided in the
 423 supplementary materials highlighting this storm evolution and CID occurrence. In the
 424 LMA source density animation, Movie S2, a lightning hole is observed between 20:50 and
 425 21:00 UTC.

426 Although the charge structure in this storm cannot be easily identified, given the
 427 low number of LMA stations, and might have been highly variable given its supercell char-

acteristics, it is clear that the much higher +CID heights are occurring in the overshooting tops, possibly above a normal upper positive charge layer, or within a top negative layer of an inverted structure. The lower number of LMA operating stations prior to 20:40 UTC unfortunately prevents a conclusive understanding of the charge structure. A number of lower-altitude -CIDs, and of even lower +CIDs, later in the storm might suggest a normal charge structure, consistent with the more common CID heights reported in the literature (e.g., Smith et al., 2004; Wu et al., 2012; Lyu et al., 2015; Zhang et al., 2016).

5.2 November 12, 2018, 13:00–15:30 UTC

In contrast to the November 10 severe storm, one of the non-severe storms of November 12 is shown in Fig. 7, a similar panel to Fig. 6. This storm occurred between 13:00–15:30 UTC moving south from near the city of Río Cuarto. Even though the storms on this day were not severe convection based on their lightning production and weaker in comparison to the storms that occurred on 10 November, there was a high variability in +CID occurrence. The case shown here is the one with the highest percentage of +CID occurrence of all observed storms, comprised of about 40% of all events with peak current higher than 10 kA, and of the highest average peak current observed in the RELAMPAGO LF lightning data. Given the energy budget of these weak storms, the extraordinarily high peak currents seen are likely due to the speed of the breakdown, while the charge transfer is actually relatively small (See Rison et al., 2016).

The more common CID height around 10 km is more prevalent in this storm as seen in Fig. 7, and on most RELAMPAGO storms excluding the cases on November 10. Nonetheless, a population of higher-altitude CIDs is still observed. Because of the large distance between this storm and the LMA, very few LMA sources are detected and they cannot provide validation of CID heights or charge layers.

Further studies are needed to understand where these high peak currents and high CID prevalence storms occur and what differentiates them from storms with less CID occurrence. Are they associated with higher IC prevalence storms, strong updrafts (Suszcynsky & Heavner, 2003), and/or geographical conditions (Sharma et al., 2008; Ahmad et al., 2010)?

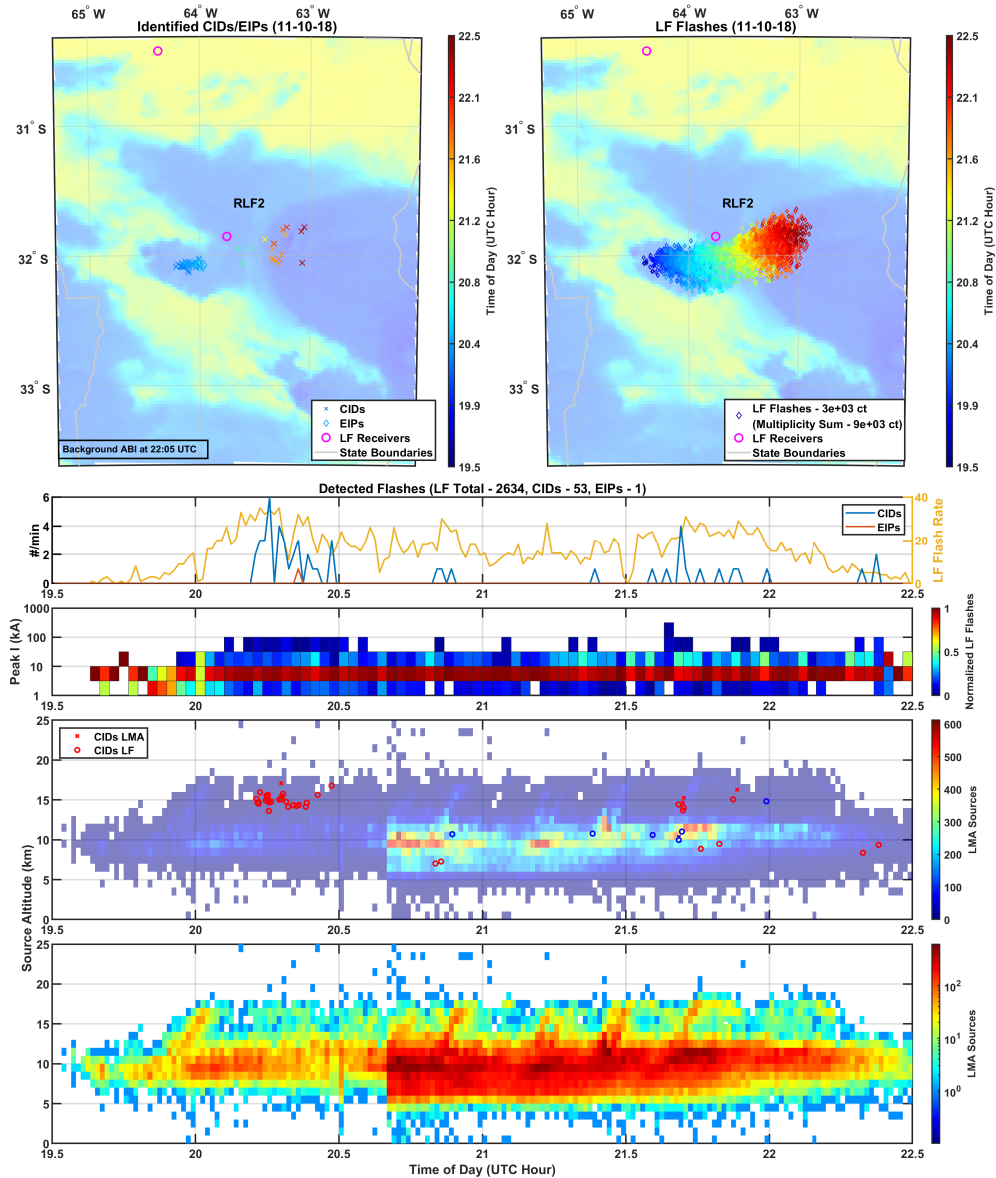


Figure 6. EIC panel displaying maps of the identified CIDs and EIP (top left), and all LF flashes (top right) for the November 10, 2018, 19:30–22:30 UTC storm near LF2. The bottom panel presents the time evolution for EICs in this storm, including EIC rates, flash peak current distribution, +CID (red) and –CID (blue) source heights (circles) and coinciding LMA source heights (crosses) within 1 ms and 25 km, on top of the distribution of all LMA source heights. The one EIP candidate identified here is actually a CG validated by CAMMA.

457

6 Summary

458

In this paper, we have investigated the classification of energetic intra-cloud (EIC)

459

lightning events during the RELAMPAGO campaign in Argentina in late 2018. The EIC

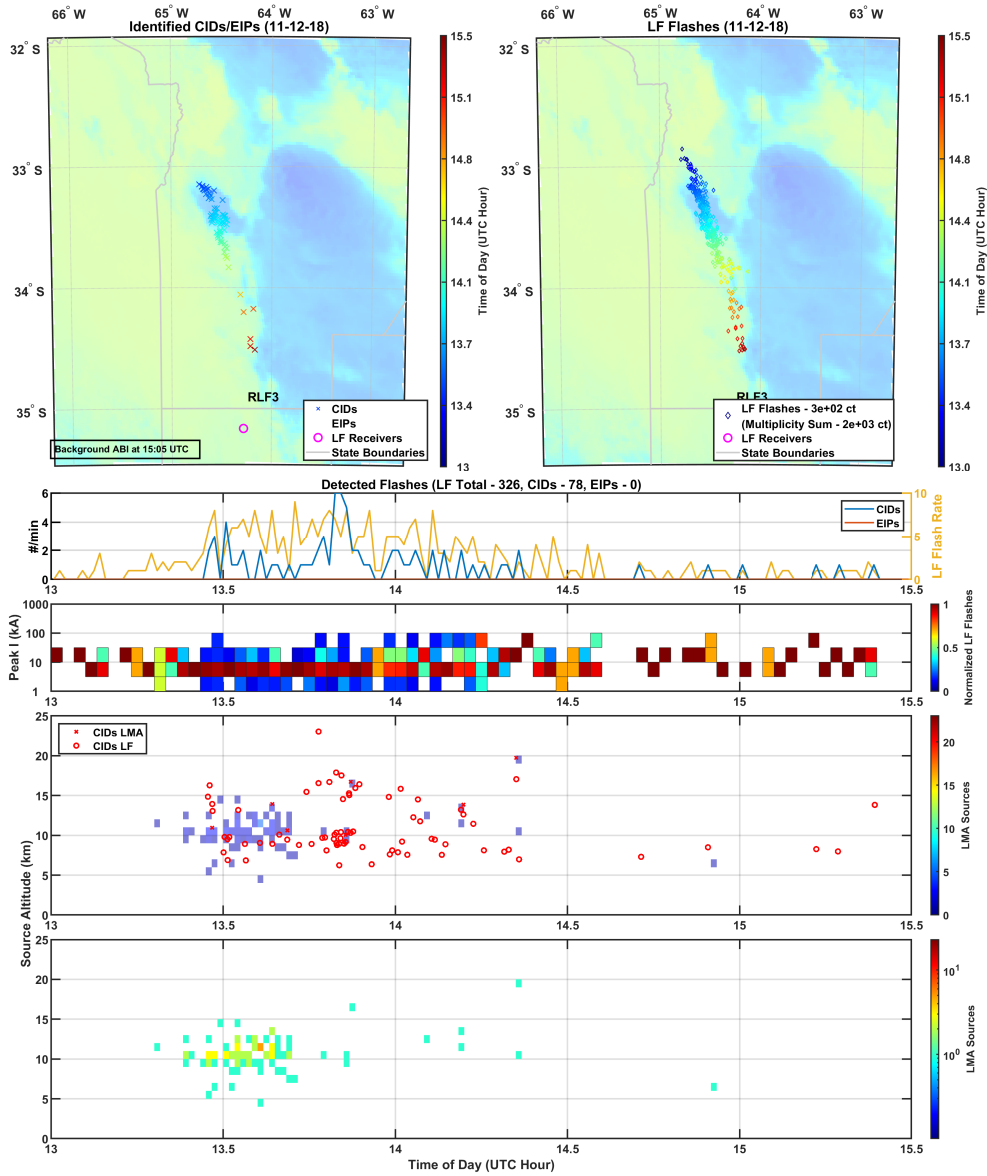


Figure 7. EIC panel displaying maps of the identified CIDs and EIP (top left), and all LF flashes (top right) for the November 12, 2018, 13:00–15:30 UTC Storm. The bottom panel presents the time evolution for EICs in this storm, including EIC rates, peak current distribution, +CID (red) and –CID (blue) source heights (circles) and coinciding LMA source heights (crosses) within 1 ms and 25 km, on top of the distribution of all LMA source heights.

460 classification implementation is described in the context of previously established research,
 461 with comprehensive details on the spheric feature identification. Similarly, an implemen-
 462 tation of EIC height estimations using skywaves was built upon established literature,

463 but additional implementation details were presented, particularly in pre-fit (innovation)
464 editing. An EIC catalog was built for the entire RELAMPAGO LF dataset, and vali-
465 dated, when possible, using other available datasets such as from LMA, CAMMA, or ENTLN.
466 A small number of high peak current events that might not have been present in the LF
467 Level 2 data were added by using ENTLN sources. The classification of CIDs proved to
468 be straightforward due to the clearly distinct population of CIDs in the classification pa-
469 rameter space, with a low number of false positives ($<3\%$). Most candidate EIPs, on the
470 other hand, did not pass manual validation. Many suffered from misidentification of their
471 sferics' main peak when the skywave merged with the groundwave for lightning sources
472 far from the receiver. Saturation heavily distorted the high peak current sources eligi-
473 ble for EIP classification. Lastly, a low number of 200+ kA events, a loose requirement
474 for EIP classification, did not provide enough samples for this study. Properties of RE-
475 LAMPAGO CIDs, both positive and negative polarity, were investigated. Those prop-
476 erties largely agree with past research on CIDs. The most striking observation was that
477 of higher altitude +CIDs than expected, for November 10, and high variability of CID
478 prevalence, as high as 40% of 10+ kA events, in ordinary storms on November 12. The
479 unusually high +CID populations on November 10 seemed to be associated with over-
480 shooting tops, but further investigation on charge structure and storm kinematics are
481 needed.

482 Using the LF EIC dataset produced and described in this paper, along with other
483 meteorological datasets, future research can address CID variability and height in RE-
484 LAMPAGO storms. In particular, future work should be aimed at understanding the
485 extreme difference in CID occurrence between non-severe storms on November 3 and 12,
486 and further investigating the supercells on November 10 with high-altitude +CIDs and
487 few -CIDs.

488 **Acknowledgments**

489 RELAMPAGO LF, LMA, ABI and GLM datasets used for this research are avail-
490 able in these in-text data citation references: (Deierling et al., 2019), user agreement re-
491 quired; (T. Lang, 2020), user agreement required; (GOES-R Calibration Working Group
492 & GOES-R Program Office, 2017), user agreement required; and (GOES-R Series Pro-
493 gram, 2019), user agreement required. ENTLN data supporting this research are avail-
494 able upon request from Earth Networks (Earth Networks, 2020), under an appropriate

495 license or user agreement, and are not accessible to the public or research community.
 496 Earth Networks customer service can be contacted to obtain licensing or user agreements.
 497 This research was supported by NSF grant AGS-1661726. AA is supported by a NASA
 498 Earth and Space Science Fellowship, grant number 80NSSC17K0392. We thank Dr. Austin
 499 Sousa for his help in servicing and deploying the LF array in RELAMPAGO. We also
 500 thank Earth Networks for providing access to the ENTLN dataset during RELAMPAGO.

501 **References**

- 502 Ahmad, N. A., Fernando, M., Baharudin, Z., Cooray, V., Ahmad, H., & Malek,
 503 Z. A. (2010, apr). Characteristics of narrow bipolar pulses observed in
 504 malaysia. *Journal of Atmospheric and Solar-Terrestrial Physics*, *72*(5-6),
 505 534–540. doi: 10.1016/j.jastp.2010.02.006
- 506 Antunes de Sá, A., Marshall, R., Sousa, A., Viets, A., & Deierling, W. (2020, nov).
 507 An array of low-cost, high-speed, autonomous electric field mills for thunder-
 508 storm research. *Earth and Space Science*, *7*(11). doi: 10.1029/2020ea001309
- 509 Antunes de Sa, A. L., Marshall, R. A., & Deierling, W. (2021). Lightning ge-
 510 olocation and flash rates from lf radio observations during the relampago
 511 field campaign. *Earth and Space Science Open Archive*, *31*. Retrieved from
 512 <https://www.essoar.org/doi/abs/10.1002/essoar.10506889.1> doi:
 513 10.1002/essoar.10506889.1
- 514 Arabshahi, S., Dwyer, J. R., Nag, A., Rakov, V. A., & Rassoul, H. K. (2014, jan).
 515 Numerical simulations of compact intracloud discharges as the relativistic run-
 516 away electron avalanche-extensive air shower process. *Journal of Geophysical*
 517 *Research: Space Physics*, *119*(1), 479–489. doi: 10.1002/2013ja018974
- 518 Carey, L., Bitzer, P., & Medina, B. (2019a). *Cordoba argentina marx meter array*
 519 *(camma) level 1 data. version 1.0*. UCAR/NCAR - Earth Observing Labora-
 520 tory. doi: 10.26023/EZ1X-DM4B-EN0V
- 521 Carey, L., Bitzer, P., & Medina, B. (2019b). *Cordoba argentina marx meter array*
 522 *(camma) level 2 data. version 1.1*. UCAR/NCAR - Earth Observing Labora-
 523 tory. doi: 10.26023/VRN7-1FJY-0X01
- 524 Cecil, D. J., & Blankenship, C. B. (2012, jan). Toward a global climatology of severe
 525 hailstorms as estimated by satellite passive microwave imagers. *Journal of Cli-*
 526 *mate*, *25*(2), 687–703. doi: 10.1175/jcli-d-11-00130.1

- 527 Cecil, D. J., Buechler, D. E., & Blakeslee, R. J. (2015, aug). TRMM LIS climatol-
 528 ogy of thunderstorm occurrence and conditional lightning flash rates. *Journal*
 529 *of Climate*, *28*(16), 6536–6547. doi: 10.1175/jcli-d-15-0124.1
- 530 Cohen, M., Inan, U., & Paschal, E. (2010, jan). Sensitive broadband ELF/VLF
 531 radio reception with the AWESOME instrument. *IEEE Transactions on Geo-*
 532 *science and Remote Sensing*, *48*(1), 3–17. doi: 10.1109/tgrs.2009.2028334
- 533 Cohen, M. B., Said, R., & Inan, U. (2010). Mitigation of 50–60 hz power line inter-
 534 ference in geophysical data. *Radio Science*, *45*(06), 1–12.
- 535 Cummer, S. A., Lyons, W. A., & Stanley, M. A. (2013, jun). Three years of light-
 536 ning impulse charge moment change measurements in the united states. *Jour-*
 537 *nal of Geophysical Research: Atmospheres*, *118*(11), 5176–5189. doi: 10.1002/
 538 jgrd.50442
- 539 Deierling, W., Marshall, R., Sá, A., & Sousa, A. (2019). *Low frequency autonomous*
 540 *magnetic field sensors (lfams) level 1 data. version 1.1.* UCAR/NCAR - Earth
 541 Observing Laboratory. doi: 10.26023/3CNH-AMVJ-B0D
- 542 Deierling, W., Marshall, R., Sá, A., & Sousa, A. (2021). *Low frequency autonomous*
 543 *magnetic field sensors (lfams) level 2 data. version 1.0.* UCAR/NCAR - Earth
 544 Observing Laboratory. doi: 10.26023/3Z4Y-BY1N-ZM0W
- 545 Eack, K. B. (2004). Electrical characteristics of narrow bipolar events. *Geophysical*
 546 *Research Letters*, *31*(20). doi: 10.1029/2004gl021117
- 547 Earth Networks. (2020). *Earth networks lightning network*. Retrieved from [https://](https://www.earthnetworks.com/why-us/networks/lightning/)
 548 www.earthnetworks.com/why-us/networks/lightning/
- 549 Franz, R. C., Nemzek, R. J., & Winckler, J. R. (1990, jul). Television image of
 550 a large upward electrical discharge above a thunderstorm system. *Science*,
 551 *249*(4964), 48–51. doi: 10.1126/science.249.4964.48
- 552 Fukunishi, H., Takahashi, Y., Kubota, M., Sakanoi, K., Inan, U. S., & Lyons,
 553 W. A. (1996, aug). Elves: Lightning-induced transient luminous events in
 554 the lower ionosphere. *Geophysical Research Letters*, *23*(16), 2157–2160. doi:
 555 10.1029/96gl01979
- 556 GOES-R Calibration Working Group, & GOES-R Program Office. (2017). *Noaa*
 557 *goes-r series advanced baseline imager (abi) level 1b radiances.* NOAA Na-
 558 tional Centers for Environmental Information. doi: 10.7289/V5BV7DSR
- 559 GOES-R Series Program. (2019). *Noaa goes-r series geostationary lightning mapper*

- 560 (*glm*) level 0 data. NOAA National Centers for Environmental Information.
561 doi: 10.25921/QC2R-PS67
- 562 Gurevich, A., Medvedev, Y., & Zybin, K. (2004, aug). New type discharge
563 generated in thunderclouds by joint action of runaway breakdown and ex-
564 tensive atmospheric shower. *Physics Letters A*, 329(4-5), 348–361. doi:
565 10.1016/j.physleta.2004.06.099
- 566 Gurevich, A. V., & Zybin, K. P. (2005, may). Runaway breakdown and the myster-
567 ies of lightning. *Physics Today*, 58(5), 37–43. doi: 10.1063/1.1995746
- 568 Heckman, S. (2014). Entln status update. In *Xv international conference on atmo-*
569 *spheric electricity* (pp. 15–20).
- 570 Inan, U. S., Bell, T. F., & Rodriguez, J. V. (1991, apr). Heating and ionization
571 of the lower ionosphere by lightning. *Geophysical Research Letters*, 18(4), 705–
572 708. doi: 10.1029/91gl00364
- 573 Inan, U. S., Cummer, S. A., & Marshall, R. A. (2010, jun). A survey of ELF and
574 VLF research on lightning-ionosphere interactions and causative discharges.
575 *Journal of Geophysical Research: Space Physics*, 115(A6), n/a–n/a. doi:
576 10.1029/2009ja014775
- 577 Lang, T. (2020). *Remote sensing of electrification, lightning, and*
578 *mesoscale/microscale processes with adaptive ground observations (relam-*
579 *pago) lightning mapper array (lma)*. NASA Global Hydrology Resource Center
580 DAAC. doi: 10.5067/RELAMPAGO/LMA/DATA101
- 581 Lang, T. J., Ávila, E. E., Blakeslee, R. J., Burchfield, J., Wingo, M., Bitzer, P. M.,
582 ... Pereyra, R. G. (2020, aug). The RELAMPAGO lightning mapping array:
583 Overview and initial comparison with the geostationary lightning mapper.
584 *Journal of Atmospheric and Oceanic Technology*, 37(8), 1457–1475. doi:
585 10.1175/jtech-d-20-0005.1
- 586 Liu, N., Dwyer, J. R., & Cummer, S. A. (2017, oct). Elves accompanying terrestrial
587 gamma ray flashes. *Journal of Geophysical Research: Space Physics*, 122(10),
588 10,563–10,576. doi: 10.1002/2017ja024344
- 589 Liu, N., Dwyer, J. R., Tilles, J. N., Stanley, M. A., Krehbiel, P. R., Rison, W., ...
590 Wilson, J. G. (2019, sep). Understanding the radio spectrum of thunder-
591 storm narrow bipolar events. *Journal of Geophysical Research: Atmospheres*,
592 124(17-18), 10134–10153. doi: 10.1029/2019jd030439

- 593 Lyu, F., & Cummer, S. A. (2018, oct). Energetic radio emissions and possible
594 terrestrial gamma-ray flashes associated with downward propagating neg-
595 ative leaders. *Geophysical Research Letters*, *45*(19), 10,764–10,771. doi:
596 10.1029/2018gl079424
- 597 Lyu, F., Cummer, S. A., Briggs, M., Marisaldi, M., Blakeslee, R. J., Bruning, E., ...
598 Stanbro, M. (2016). Ground detection of terrestrial gamma ray flashes from
599 distant radio signals. *Geophysical Research Letters*, *43*(16), 8728–8734. doi:
600 10.1002/2016gl070154
- 601 Lyu, F., Cummer, S. A., Krehbiel, P. R., Rison, W., Briggs, M. S., Cramer, E., ...
602 Stanbro, M. (2018, feb). Very high frequency radio emissions associated with
603 the production of terrestrial gamma-ray flashes. *Geophysical Research Letters*,
604 *45*(4), 2097–2105. doi: 10.1002/2018gl077102
- 605 Lyu, F., Cummer, S. A., & McTague, L. (2015). Insights into high peak current
606 in-cloud lightning events during thunderstorms. *Geophysical Research Letters*,
607 *42*(16), 6836–6843. doi: 10.1002/2015gl065047
- 608 Marshall, R. A. (2012, mar). An improved model of the lightning electromagnetic
609 field interaction with the d-region ionosphere. *Journal of Geophysical Research:*
610 *Space Physics*, *117*(A3), n/a–n/a. doi: 10.1029/2011ja017408
- 611 Marshall, R. A., da Silva, C. L., & Pasko, V. P. (2015). Elve doublets and compact
612 intracloud discharges. *Geophysical Research Letters*, *42*(14), 6112–6119. doi:
613 10.1002/2015gl064862
- 614 Nag, A., & Rakov, V. A. (2010). Compact intracloud lightning discharges: 1. mech-
615 anism of electromagnetic radiation and modeling. *Journal of Geophysical Re-*
616 *search*, *115*(D20). doi: 10.1029/2010jd014235
- 617 Nesbitt, S. (2020). *Relampago-cacti*. Retrieved from [https://sites.google.com/
618 illinois.edu/relampago/home](https://sites.google.com/illinois.edu/relampago/home)
- 619 Orville, R. E. (1991). Calibration of a magnetic direction finding network using mea-
620 sured triggered lightning return stroke peak currents. *Journal of Geophysical*
621 *Research*, *96*(D9), 17135. doi: 10.1029/91jd00611
- 622 Rasmussen, K. L., Zuluaga, M. D., & Houze, R. A. (2014, oct). Severe convec-
623 tion and lightning in subtropical south america. *Geophysical Research Letters*,
624 *41*(20), 7359–7366. doi: 10.1002/2014gl061767
- 625 Rison, W., Krehbiel, P. R., Stock, M. G., Edens, H. E., Shao, X.-M., Thomas, R. J.,

- 626 ... Zhang, Y. (2016, feb). Observations of narrow bipolar events reveal how
627 lightning is initiated in thunderstorms. *Nature Communications*, 7(1). doi:
628 10.1038/ncomms10721
- 629 Rison, W., Thomas, R. J., Krehbiel, P. R., Hamlin, T., & Harlin, J. (1999, dec). A
630 GPS-based three-dimensional lightning mapping system: Initial observations
631 in central new mexico. *Geophysical Research Letters*, 26(23), 3573–3576. doi:
632 10.1029/1999gl010856
- 633 Sharma, S., Fernando, M., & Cooray, V. (2008, jul). Narrow positive bipolar radi-
634 ation from lightning observed in sri lanka. *Journal of Atmospheric and Solar-
635 Terrestrial Physics*, 70(10), 1251–1260. doi: 10.1016/j.jastp.2008.03.002
- 636 Smith, D. A., Eack, K. B., Harlin, J., Heavner, M. J., Jacobson, A. R., Massey,
637 R. S., ... Wiens, K. C. (2002). The los alamos sferic array: A research
638 tool for lightning investigations. *Journal of Geophysical Research: At-
639 mospheres*, 107(D13), ACL 5-1-ACL 5-14. Retrieved from [https://](https://agupubs.onlinelibrary.wiley.com/doi/abs/10.1029/2001JD000502)
640 agupubs.onlinelibrary.wiley.com/doi/abs/10.1029/2001JD000502 doi:
641 <https://doi.org/10.1029/2001JD000502>
- 642 Smith, D. A., Heavner, M. J., Jacobson, A. R., Shao, X. M., Massey, R. S., Shel-
643 don, R. J., & Wiens, K. C. (2004, feb). A method for determining intracloud
644 lightning and ionospheric heights from VLF/LF electric field records. *Radio
645 Science*, 39(1), n/a–n/a. doi: 10.1029/2002rs002790
- 646 Smith, D. A., Shao, X. M., Holden, D. N., Rhodes, C. T., Brook, M., Krehbiel,
647 P. R., ... Thomas, R. J. (1999a). A distinct class of isolated intracloud light-
648 ning discharges and their associated radio emissions. *Journal of Geophysical
649 Research: Atmospheres*, 104(D4), 4189–4212. doi: 10.1029/1998jd200045
- 650 Suszcynsky, D. M., & Heavner, M. J. (2003, sep). Narrow bipolar events as indi-
651 cators of thunderstorm convective strength. *Geophysical Research Letters*,
652 30(17), n/a–n/a. doi: 10.1029/2003gl017834
- 653 Tilles, J. N., Krehbiel, P. R., Stanley, M. A., Rison, W., Liu, N., Lyu, F., ... Wil-
654 son, J. (2020, oct). Radio interferometer observations of an energetic in-cloud
655 pulse reveal large currents generated by relativistic discharges. *Journal of
656 Geophysical Research: Atmospheres*, 125(20). doi: 10.1029/2020jd032603
- 657 Tilles, J. N., Liu, N., Stanley, M. A., Krehbiel, P. R., Rison, W., Stock, M. G., ...
658 Wilson, J. (2019, apr). Fast negative breakdown in thunderstorms. *Nature*

- 659 *Communications*, 10(1). doi: 10.1038/s41467-019-09621-z
- 660 Vine, D. M. L. (1980). Sources of the strongest RF radiation from lightning. *Journal*
661 *of Geophysical Research*, 85(C7), 4091. doi: 10.1029/jc085ic07p04091
- 662 Watson, S. S., & Marshall, T. C. (2007). Current propagation model for a nar-
663 row bipolar pulse. *Geophysical Research Letters*, 34(4). doi: 10.1029/
664 2006gl027426
- 665 Willett, J. C., Bailey, J. C., & Krider, E. P. (1989). A class of unusual lightning
666 electric field waveforms with very strong high-frequency radiation. *Journal of*
667 *Geophysical Research*, 94(D13), 16255. doi: 10.1029/jd094id13p16255
- 668 Wu, T., Dong, W., Zhang, Y., Funaki, T., Yoshida, S., Morimoto, T., . . . Kawasaki,
669 Z. (2012, mar). Discharge height of lightning narrow bipolar events.
670 *Journal of Geophysical Research: Atmospheres*, 117(D5), n/a–n/a. doi:
671 10.1029/2011jd017054
- 672 Wu, T., Dong, W., Zhang, Y., & Wang, T. (2011, feb). Comparison of positive
673 and negative compact intracloud discharges. *Journal of Geophysical Research*,
674 116(D3). doi: 10.1029/2010jd015233
- 675 Zhang, H., Lu, G., Qie, X., Jiang, R., Fan, Y., Tian, Y., . . . Feng, G. (2016,
676 jun). Locating narrow bipolar events with single-station measurement of
677 low-frequency magnetic fields. *Journal of Atmospheric and Solar-Terrestrial*
678 *Physics*, 143–144, 88–101. doi: 10.1016/j.jastp.2016.03.009
- 679 Zhu, Y., Bitzer, P., Stewart, M., Podgorny, S., Corredor, D., Burchfield, J., . . .
680 Stock, M. (2020, apr). Huntsville alabama marx meter array 2: Upgrade and
681 capability. *Earth and Space Science*, 7(4). doi: 10.1029/2020ea001111
- 682 Zipser, E. J., Cecil, D. J., Liu, C., Nesbitt, S. W., & Yorty, D. P. (2006, aug).
683 WHERE ARE THE MOST INTENSE THUNDERSTORMS ON EARTH?
684 *Bulletin of the American Meteorological Society*, 87(8), 1057–1072. doi:
685 10.1175/bams-87-8-1057